13th World Conference on Earthquake Engineering
Vancouver, B.C., Canada
August 1-6, 2004
Paper No. 2816

FINITE ELEMENT MODELING OF CONCENTRICALLY BRACED FRAMES FOR EARTHQUAKES

Madhar Haddad[1], Tom Brown[2], Nigel Shrive[3]

SUMMARY

Braced frames construction, while having advantage in reducing earthquakes induced displacements, is susceptible to loss of ductility attributed to brace behaviour. A numerical model has been developed that is capable of accurately simulating the hysteresis behaviour of bracing members. The factors that affect that behaviour can therefore be studied without conducting expensive experimental tests. The three-dimensional nonlinear elasto-plastic finite element model has been used to simulate the behaviour of hollow structural steel tubes connected to gusset plates at their ends when subjected to reversed axial displacements. A combined orthotropic kinematic hardening material model was used. Four-node finite membrane strain quadrilateral shell elements were used to model both the HSS and the gusset plate. Fixed boundary conditions were applied at the ends of the specimens with axial displacements imposed for each cycle. The model was able to simulate the hysteresis behaviour of experimentally tested bracing members through the peak loads and displacements, the degradation of both strength and stiffness and the energy dissipation.

[1] PhD Candidate, Department of Civil Engineering, University of Calgary, 2500 University Drive NW, Calgary, AB, Canada, T2N 1N4 (mahaddad@ucalgary.ca), Phone: (403) 210-7356.
[2] Professor and Head, Department of Civil Engineering, University of Calgary, 2500 University Drive NW, Calgary, AB, Canada, T2N 1N4 (brownt@ucalgary.ca)
[3] Professor, Department of Civil Engineering, University of Calgary, 2500 University Drive NW, Calgary, AB, Canada, T2N 1N4 (shrive@ucalgary.ca)

INTRODUCTION

In addition to the strength and lateral stiffness that bracing members provide to braced steel frames, bracing members are a primary source of energy dissipation during earthquakes. Energy is dissipated through the post-buckling and yielding hysteresis behaviour of steel bracing members and this energy is a significant parameter with respect to the survival of the braced frame. Though steel tubular members are susceptible to local buckling and residual elongation, which result in deterioration of buckling capacity, they are highly efficient structural members for dissipating energy.

Many factors have been shown to affect fracture life of the member, including the width-to-thickness ratio, the effective slenderness ratio, the width-to-depth ratio, and the mechanical properties of the steel. Shaback [1] conducted a series of experimental tests involving cyclic loading of cold-formed square hollow steel sections (HSS) connected to hot-rolled steel gusset plates. The effective length factor was calculated according to the formula presented by Jain et al. [2]. All specimens were designed to the requirements of CAN/CSA-S16.1-94 Clause 27.4 [3] for the design of diagonal members and bracing connections for ductile concentrically braced frames with the exception of the connection weld. The Shaback results, used to verify the finite element model developed here, showed that most specimens failed after approximately ten cycles of inelastic buckling. The free length of the gusset plates ranged between 1.25 to 2.0 times their thicknesses. Astaneh-Asl et al [4] suggested that the free length should be twice the thickness of the gusset, such that the location and magnitude of plastic hinges formed at the ends of the brace were predictable.

Cheng et al [5] presented an experimental program and associated numerical analysis to study the shear-lag effect in round HSS tension members welded to gusset plates at their ends. A critical equivalent strain limit was assumed to define material failure in their numerical analysis, with which they were able to predict the magnitude of the peak load and the location of fracture.

Goel (Jain et al, [6]; Astaneh-Asl and Goel, [7]; Astaneh-Asl et al, [4]) has conducted the most extensive research program in this area. The behaviour of double-angle bracing members subjected to in-plane and out-of-plane buckling due to cyclic loading reversals was investigated experimentally (Astaneh-Asl and Goel, [7]; Astaneh-Asl et al, [4]). The residual elongation and the reduction in the maximum compressive strength of tube specimens as a function of the number of loading cycles were also investigated (Jain et al, [6]). Four of Goel's conclusions are: (a), the buckling load capacity of bracing members decreases during cyclic loading; (b), three plastic hinges generally form in the bracing member, one at mid-length, and the other two at the ends; (c), the flexural strength of the gusset plates should be kept smaller than that of the member in order to avoid biaxial buckling and consequent cracking of the welds between the member and the gusset plate; and (d), connection details and the mode of buckling do not influence the hysteresis curve.

Goel's conclusions indicate that there are numerous parameters which can affect the energy dissipation capacity of a steel bracing member. However, little has been done to evaluate or understand how these parameters interact with each other or individually affect brace capacity. Research to date has been based on either experimental or non-general phenomenological models. There therefore appears to be a need to create a general three-dimensional non-linear elasto-plastic finite element model, verified by reliable experimental data, to simulate the hysteresis behaviour of cold-formed steel braces subject to cyclic loadings. A three dimensional non-linear elastic plastic finite element model using Abaqus, version 5.8 (Hibbitt, Karlsson & Sorensen Inc. [8]) with Patran and Abaqus Post as pre and post processors respectively, has been developed to simulate the cyclic behaviour of HSS sections with rectangular gusset plates at their ends.

FINITE ELEMENT MODEL

Four node quadrilateral shell elements were used in the model. The formulation of these elements accounts for finite membrane strains and rotations, and allows for changes in thickness with deformation.

Fixed boundary conditions were applied at the ends of the specimens with displacements imposed to control the deformation extent of each cycle. The gusset plates were assumed to be connected perfectly to the HSS as shown in Figure 1. The modulus of elasticity of the steel was taken as 200 GPa, complying with the CSA G40.21 350W standard. By invoking symmetry, only half of the specimen was modeled.

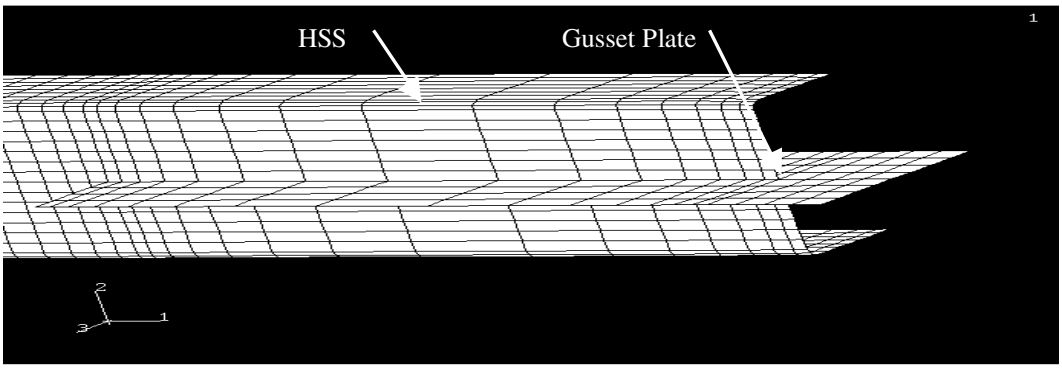

Figure 1: Connection between the HSS and the Gusset Plate

The objective of the analysis was to determine the nonlinear load displacement curve for the specimens when subjected to cyclic axial deformation. Each defined step involves nonlinear analysis using the full Newton method. Each step is subsequently divided into small linear steps so that the non-linear stress strain relationship can be followed. An initial increment is suggested and Abaqus automatically chooses the size of the following increments. Within each increment, iteration is used to find the equilibrium solution. At the end of each increment the solution attains equilibrium to some specified tolerance.

The finite element models by Rabinovitch and Cheng [9], Walbridge et al. [10] and Nast et al. [11] used an isotropic hardening material model to simulate the change in plastic behaviour of the steel during the cyclic loading. The isotropic model changes the yield surface size equally in all directions in stress space so that the yield stress decreases or increases equally in all stress directions as plastic straining occurs. A standard von Mises yield function with associated plastic flow rule was used in the isotropic hardening model. Therefore, as the material yields, the inelastic deformation rate is in the direction normal to the yield surface at the location corresponding to the current yield stress state. While this model is generally accepted and used for most analyses with metals, it is not able to simulate the actual shift in the yield

surface. Directionality develops in the zone of plasticity in the plastic hinge, and with the subsequent strain hardening, the plasticity that actually occurs tends to be orthotropic.

In modeling cyclic loading reversals of axially loaded members, a combined orthotropic kinematic hardening model is more appropriate. This model is capable of simulating the expansion and contraction of the yield surface through an orthotropic hardening model, but also models the shift of the yield surface through kinematic hardening to account for the Bauschinger effect. The model uses the Hill criterion [12] (an expansion of the von Mises criterion) to simulate orthotropy.

The finite element analysis was performed in two stages. The first analysis was conducted to create a small camber in the specimens to match the measured camber in the test specimens. An initial imperfection is necessary to make the specimen buckle in the second analysis, involving the applied axial displacements.

ANALYSIS AND DISCUSSION OF RESULTS

Two HSS brace specimens with end connections (Table 1) were analyzed using the finite element model discussed above and were compared to the corresponding specimens tested in the laboratory. The axial displacements were applied in an increasing sequence starting with compression loading (Shaback [1]).

Table 1: Specimens Geometric Properties

Specimen	HSS		Gusset Plate				Specimen		
	Section (mm)	Length (mm)	Length (mm)	Width (mm)	Thickness (mm)	Free Length (mm)	KL/r	W/t	Initial Camber (mm)
1	127x127x8	3350	351	225	25.4	51	53.9	12.9	0.04
2	152x152x8	3950	395	250	25.4	45	53.3	16.0	1.45

Specimen 1

The experimental and the equivalent numerical axial hysteresis loops are shown in Figure 2. Load cycles are clockwise in the diagram. The specimen was subjected to two initial cycles of elastic loading

beginning in compression followed by two partial yielding cycles. During the fifth compressive cycle the specimen buckled under a compressive load of 1156 kN. The HSS fully yielded on the tension side of the sixth cycle at a load of 1647 kN. The degradation of the axial compression capacity is clearly seen from the hysteresis curves with each subsequent cycle. During the ninth cycle, the specimen buckled locally at the mid-span at a value of approximately 35 mm axial displacement. A noticeable residual lateral deflection remained in the specimen upon reloading in tension for each cycle. Loading continued with increasing local buckling at the specimen mid-span. In the tensile portion of the eleventh cycle, the HSS specimen failed. Plastic hinges formed in the end connections first with the third, mid-span plastic hinge, forming later.

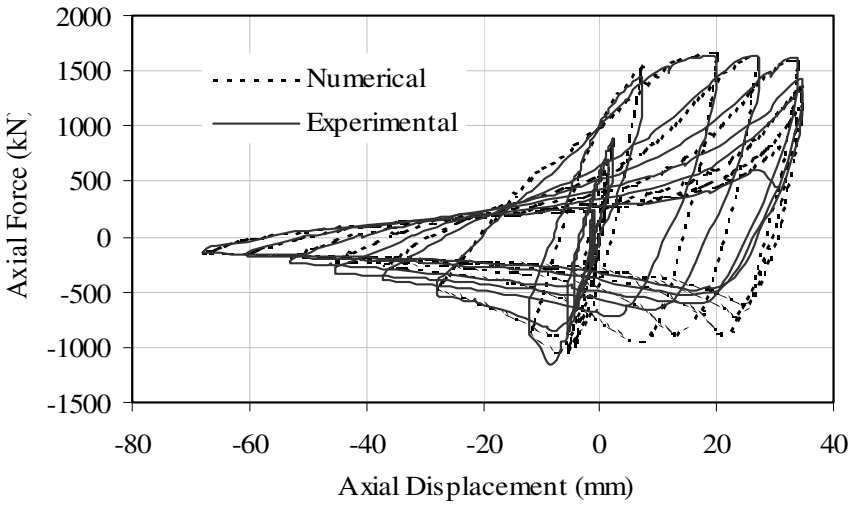

Figure 2: Axial Hysteresis Loops for Specimen 1

Specimen 2

The experimental and the equivalent numerical axial hysteresis loops are shown in Figure 3. After two initial cycles of elastic loading the specimen were subjected to two cycles that partially yielded the specimen. Specimen 2 buckled at a compressive load of 1507 kN. The HSS yielded on the tension side of the sixth cycle at a maximum load of 2165 kN. The subsequent degradation of the axial compression load capacity, similar to specimen 1, is seen from the hysteresis curves with subsequent cycles. On the eighth cycle, the specimen buckled locally at the mid-span at a value of approximately 25 mm axial

displacement. As with the first specimen, there was noticeable residual lateral deflection upon reloading in tension for the next cycle. Failure occurred in the tension portion of the ninth cycle. As with the first specimen, plastic hinges formed in the end connections first, followed by the third mid-span plastic hinge.

The different size specimens (Specimen 1 and 2) had approximately the same slenderness ratio. However the width to thickness ratio of the second specimen was larger than that of the first. This results in the earlier fracture of the second specimen.

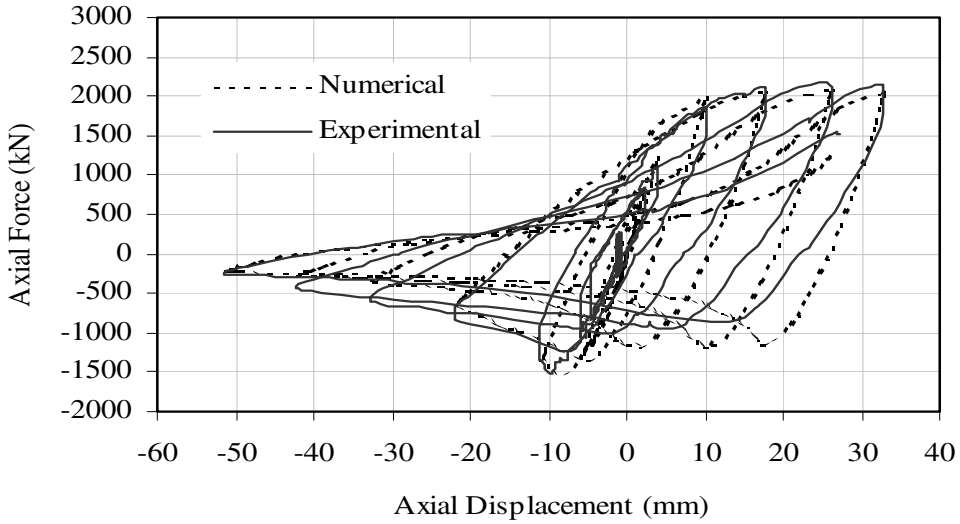

Figure 3: Axial Hysteresis Loops for Specimen 2

The bulging of the specimens at mid-span and the cumulative plastic strain localization are illustrated in Figure 4. In the finite element model, the same number of nodes and elements (mesh) were used in both specimens. The local mesh density was increased gradually toward the expected plastic hinge locations (at the free end of the gusset plates and at the middle of the specimens). The experimental and numerical stationary test points are summarized in Table 2.

The general appearance of axial and lateral hysteresis loops reveals that the accuracy of the finite element model is excellent. Comparisons of numerical/ experimental results in terms of strength, stiffness, out-of-plane displacements, and energy dissipation are presented below.

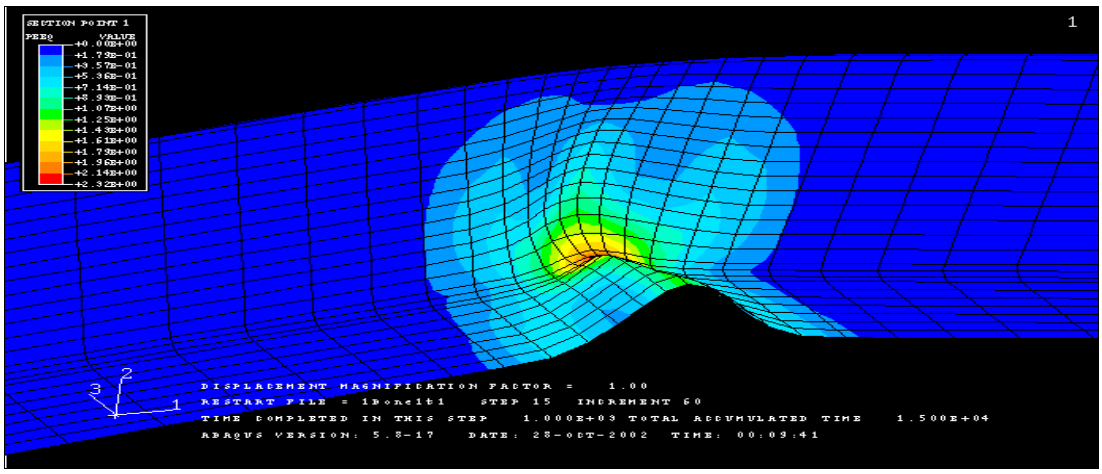

Figure 4: Mid-Length Plastic Hinge

Table 2: Experimental Versus Numerical Stationary Test Points

Variables	Specimen 1			Specimen 2		
	Experimental	Numerical	Error %	Experimental	Numerical	Error %
Buckling Capacity (kN)	1159	1051	9.3	1507	1508	0.0
Tensile Resistance (kN)	1647	1678	1.9	2165	2080	3.9
Initial Buckling Cycle	5	5	0.0	5	5	0.0
First Local Buckling Cycle	9	9	0.0	8	8	0.0
Cumulative Plastic Strain	N.A.	7.08	N.A.	N.A.	3.99	N.A.
Fracture Cycle	11	N.A.	N.A.	9	N.A.	N.A.
Energy Dissipation (N.m)	357000	362000	1.4	300000	283000	5.7

A. STRENGTH

The experimental and numerical axial hysteresis envelopes are shown in Figures 5 and 6, respectively. The S-shape envelopes are plots of the maximum axial displacements versus the maximum axial loads for all tension and compression cycles. The upper portion of the S curve, in the first quadrant (positive displacements/ positive axial loads), is the tension envelope and the lower portion of the S curve, in the

third quadrant (negative displacements/ negative axial loads), is the compression envelope. Hysteresis envelopes can be categorized as either elastic envelopes or inelastic (buckling or yielding) envelopes. In both tests, the envelopes start as elastic, and became inelastic when the brace buckled in compression or yielded in tension. During the first buckling, and the following cycles, the degradation in the compressive capacity can be seen in the third quadrant of the figures. The tensile capacity remains approximately constant, with no significant strain hardening occurring.

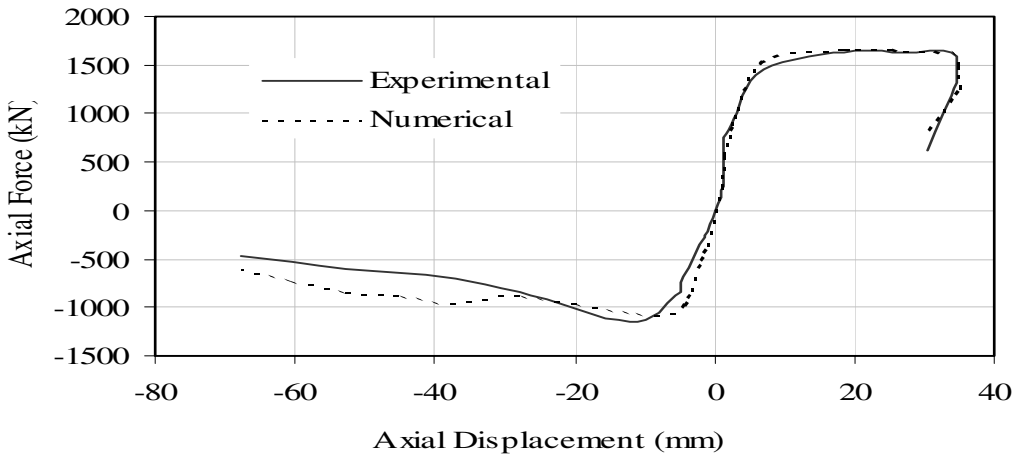

Figure 5: Axial Hysteresis Envelopes for Specimen 1

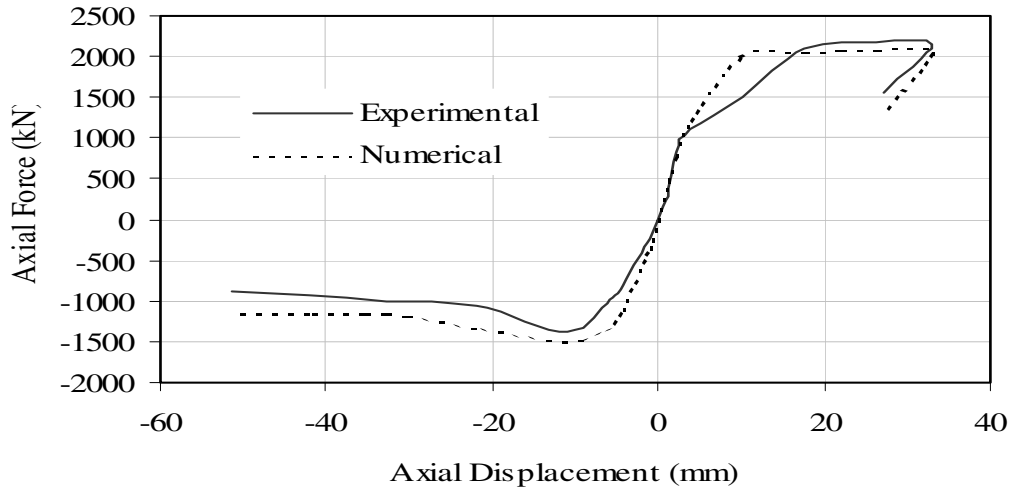

Figure 6: Axial Hysteresis Envelopes for Specimen 2

B. STIFFNESS

The degradation of both the experimental and the numerical stiffness is seen from the axial hysteresis loops, shown in Figures 2 and 3. The degradation of the experimental and numerical axial stiffnesses at

zero axial displacement when transferring from compression unloading to tension loading and vice versa are listed in Table 3, for specimen 1. Good agreement between experimental and numerical values of stiffnesses is observed during all cycles when transferring from compression unloading to tension loading. The experimental and numerical stiffnesses diverge when transferring from tension unloading to compression loading. The stiffness of the axial hysteresis loops significantly dropped from 200 GPa during the first cycle to 7.8 GPa during the eleventh cycle, when transferring from compression unloading to tension loading.

Table 3: Experimental Versus Numerical Axial Stiffness at Zero Axial Displacement for Specimen 1

Cycle No.	Axial Stiffness (GPa)					
	Compression to Tension			Tension to Compression		
	Experimental	Numerical	ERROR %	Experimental	Numerical	ERROR %
1	198.3	200	0.9	197.1	200	1.5
2	198.3	200	0.9	196.6	200	1.7
3	191.2	198.7	3.9	194.1	197.6	1.8
4	187.0	192.7	3.0	190.3	196.4	3.2
5	76.2	84.2	10.5	142.5	183.3	28.6
6	53.2	57.14	7.4	121.6	174.2	43.3
7	30.6	32.3	5.6	100.2	169.9	69.6
8	25.3	22.5	11.1	95.3	167.7	76.0
9	16.7	19.4	16.2	93.8	166.3	77.3
10	12.7	12.7	0.0	91.9	165.2	79.8
11	7.8	7.9	1.3	---------	--------	-------

C. OUT-OF-PLANE DISPLACEMENT

The experimental and numerical lateral hysteresis envelopes for specimens 1 and 2 are shown in Figures 7 and 8, respectively. Good agreement in both the behaviour and the values is clearly seen. The out-of-plane tension and compression displacements are located in the first (positive lateral displacement/ positive axial load) and fourth (positive lateral displacement/ negative axial load) quadrants, respectively. The specimens were all tested with the fabrication camber set in the same direction so only positive lateral deflection occurs. The lateral displacement in both tension and compression is equal to zero until the first compressive buckling cycle. Thereafter, the compressive out-of-plane displacement increases during all

the compressive cycles. The rate of increase decreases if the axial compressive displacement is limited by the stroke capacity.

The lateral tension displacement starts to diverge from zero during the tension side of the cycles following the first compressive buckling cycle. This increase in the lateral displacement is due to the residual elongation (column growth) of the brace, which in turn is a result of the inelastic behaviour (yielding and buckling) of the bracing member.

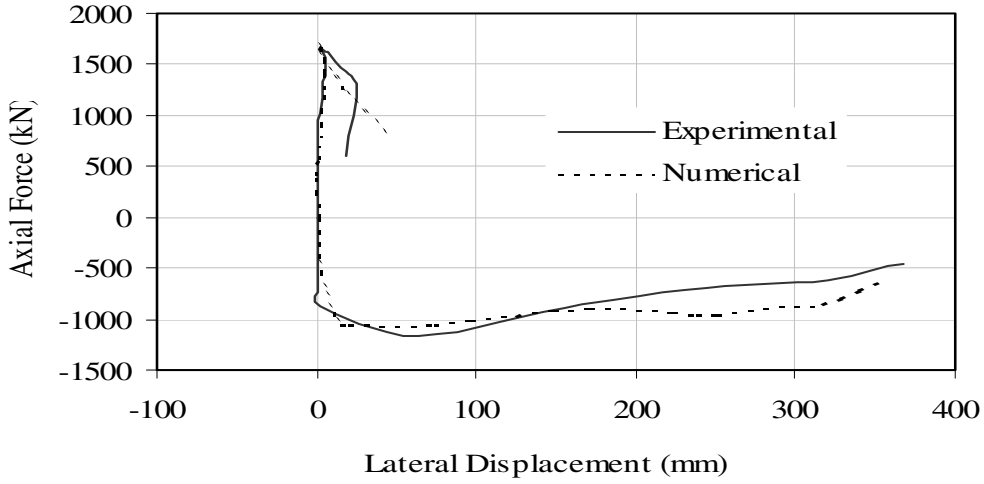

Figure 7: Lateral Hysteresis Envelopes for Specimen 1

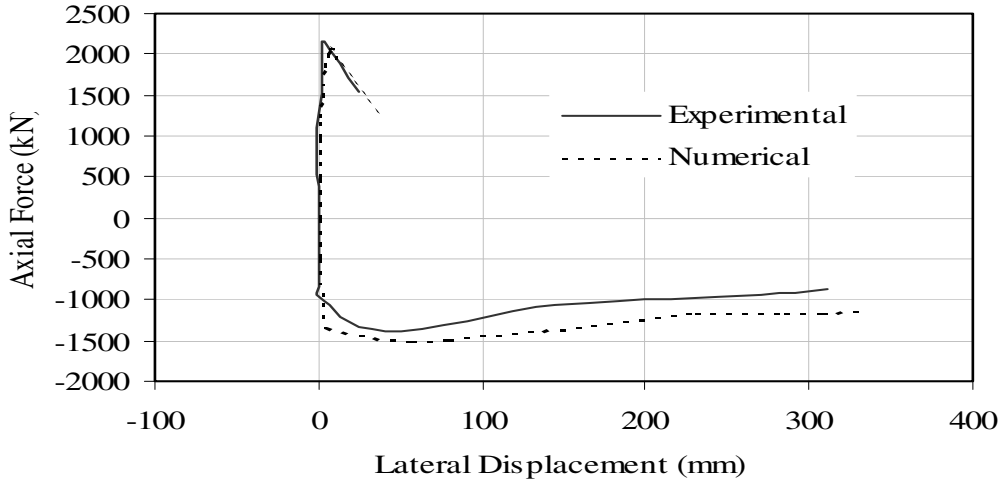

Figure 8: Lateral Hysteresis Envelopes for Specimen 2.

The degradation of the tensile resistance during the last cycle, when the specimens fracture, is seen from the lateral hysteresis envelopes. 50% of the mid-length cross-section has fractured at tensile loads lower than the tensile resistance, while the specimens were still bent.

D. ENERGY DISSIPATION

The area under the axial hysteresis loops represents the energy dissipation capacity of the brace during the load reversals; this is an important attribute during earthquake ground motion. The experimental, and corresponding numerical, energy absorbed per cycle versus cycle number is shown in Figures 9 and 10. The experimental and the numerical cumulative energy dissipations for both specimens are listed in Table 1. The energy absorbed is equal to zero during the first two (elastic) cycles. A slight increase in the energy dissipation, not exceeding 5000 N.m, occurs during the each of the partial yielding cycles (cycles 3 and 4).

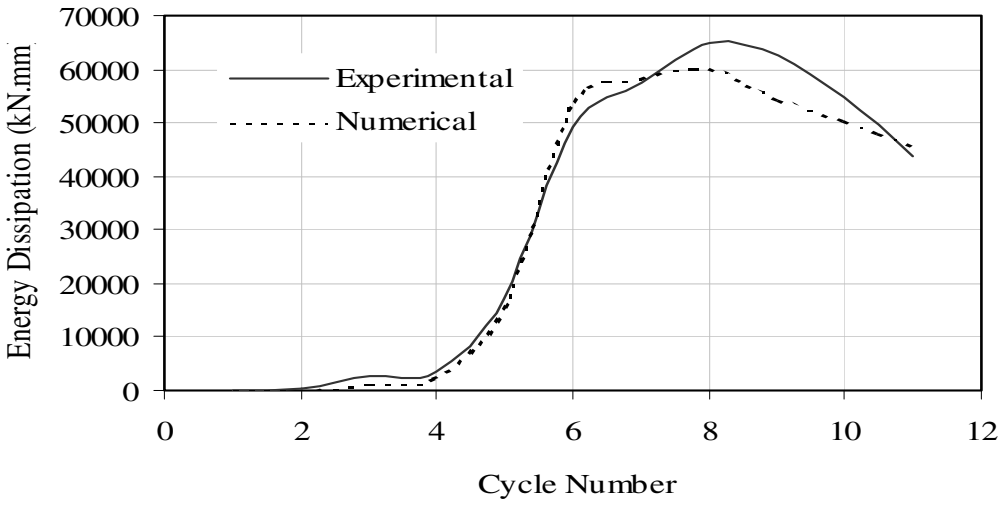

Figure 9: Variation of Energy Dissipation with Cycle Number for Specimen 1

A significant increase in the rate of energy dissipation occurs thereafter, due to buckling and yielding of the bracing member. However, the rate of the energy dissipation starts to decline and degrades rapidly during the last cycles. The degradation is due to the reduction of both the strength and the stiffness of the brace, due to local buckling and the Bauschinger effect. The degradation starts early in specimen 1 due to the severity of the local buckling.

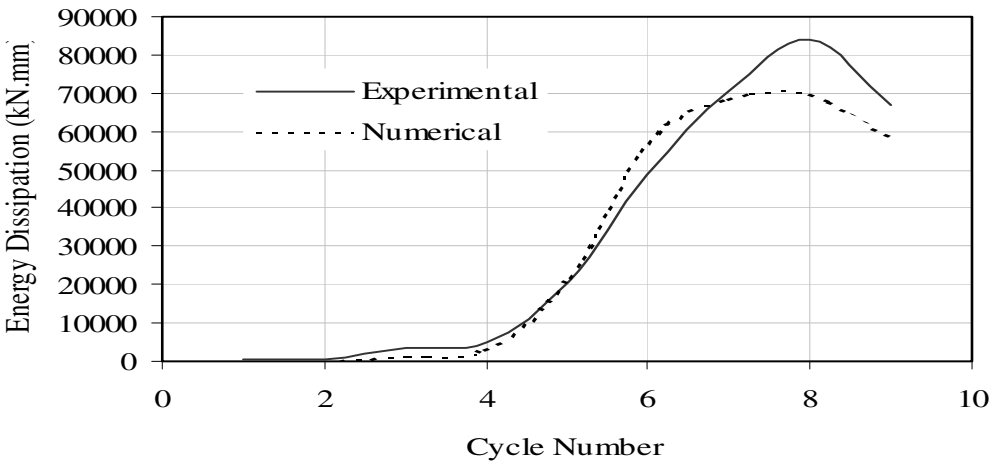

Figure 10: Variation of Energy Dissipation with Cycle Number for Specimen 2

This numerical model demonstrates that it is possible to simulate the energy dissipation characteristics of axially loaded HSS bracing members. The model can therefore be used to investigate the effects of some of the geometric parameters on the behaviour of axially loaded HSS sections. As demonstrated here for example, a free length of only 1.25 times the gusset plate thickness is sufficient for the formation of plastic hinges at the ends of the specimen for the materials used in Shaback's experiments.

CONCLUSIONS

1. The finite element model described is capable of representing the cyclic behaviour of cold-formed hollow structural steel sections connected to gusset plates at their ends in terms of strength, stiffness, out-of-plane displacement, and energy dissipation.

2. The combined orthotropic kinematic hardening material model is more appropriate than the isotropic hardening material model in simulating the behaviour of HSS braces under cyclic loading.

3. A gusset plate free length of 1.25 its thickness is sufficient for the formation of plastic hinges at the ends of the specimens modelled here.

ACKNOWLEDGEMENTS

The authors gratefully acknowledge the financial support of the Steel Structures Education Foundation, TSE Steel Ltd. and the Natural Sciences and Engineering Research Council of Canada for this work. Special thanks goes to Dr. Doug Phillips for his assistant in the finite element analysis.

REFERENCES

1. Shaback. B. "HSS brace behaviour under cyclic loading." M.S. Thesis, Department of Civil Engineering, University of Calgary, Calgary, Alberta, 2001: 49-100.
2. Jain, A.K., Goel, S.C., and Hanson, R.D. "Inelastic response of restrained steel tubes." Journal of Structural Division, ASCE, 1978: 104(6): 897-910.
3. CSA. "Limit State Design of Steel Structures." CAN/CSA-S16.1-94. Canadian Standards Association, Rexdale, Ontario. 1994.
4. Astaneh-Asl, A., Goel, S.C., and Hanson, R.D. "Cyclic out-of-plane buckling of double angle bracing." Journal of Structural Engineering, ASCE, 1985: 111(5): 1135-1153.
5. Cheng, J.J.R., Kalak, G.L., and Khoo, H. "Strength of slotted tubular tension members." Canadian Journal of Civil Engineering, 1998: 25(6): 982-991.
6. Jain, A.K., Goel, S.C., and Hanson, R.D. "Hysteretic cycles of axially loaded steel members." Journal of Structural Division, ASCE, 1980: 106(ST8): 1777-1795.
7. Astaneh-Asl A., Goel S.C. "Cyclic in-plane buckling of double angle braces." Journal of Structural Engineering, ASCE, 1984: 110(9): 2036-2055.
8. Hibbitt, Karlsson & Sorensen Inc, "ABAQUS/ standard user's manual." Version 5.8. Hibbitt, Karlsson &Sorensen Inc., Pawtucket, R.I. 1994, Vols. 1 and 2.
9. Rabinovitch, J.S., and Cheng, J.J.R. "Cyclic behaviour of steel gusset plate connections." Structural Engineering Report no. 191, Department of Civil Engineering, University of Alberta, Edmonton, Alberta. 1993.

10. Walbridge, S.S., Grondin, G.Y., and Cheng, J.J. “An analysis of the cyclic behaviour of steel gusset plate connections.” Structural Engineering Report No. 225, Department of Civil Engineering, University of Alberta, Edmonton, Alberta. 1998.
11. Nast, T.E., Grondin, G.Y., and Cheng, J.J.R. “Cyclic behaviour of stiffened gusset plate- brace member assemblies.” Structural Engineering Report No. 229, Department of Civil Engineering, University of Alberta, Edmonton, Alberta. 1999.
12. Hill, R. “The mathematical theory of plasticity.” New York: Oxford University Press, 1950.